Eur. Phys. J. C (2021) 81:687
https://doi.org/10.1140/epjc/s10052-021-09470-5

THE EUROPEAN PHYSICAL JOURNAL C

Regular Article - Theoretical Physics

Four-lepton production in gluon fusion at NLO matched to parton showers

Simone Alioli[1,a], **Silvia Ferrario Ravasio**[2,3,b], **Jonas M. Lindert**[4,c], **Raoul Röntsch**[5,d]

[1] Università degli Studi di Milano-Bicocca, INFN, Piazza della Scienza 3, Milan 20126, Italy
[2] Rudolf Peierls Centre for Theoretical Physics, University of Oxford, Parks Road, Oxford OX1 3PU, UK
[3] IPPP, Department of Physics, Durham University, Durham DH1 3LE, UK
[4] Department of Physics and Astronomy, University of Sussex, Brighton BN1 9QH, UK
[5] Theoretical Physics Department, CERN, 1211 Geneva 23, Switzerland

Received: 1 April 2021 / Accepted: 21 July 2021 / Published online: 3 August 2021

Abstract We present a calculation of the next-to-leading order (NLO) QCD corrections to gluon-induced electroweak gauge boson pair production, $gg \to ZZ$ and $gg \to W^+W^-$, matched to the PYTHIA 8 parton shower in the POWHEG approach. The calculation consistently incorporates the continuum background, the Higgs-mediated $gg \to H^* \to VV$ process, and their interference. We consider leptonic decay modes of the vector bosons and retain offshell and non-resonant contributions. The processes considered are loop-induced at leading order and thus contain two-loop virtual contributions as well as loop-squared real contributions. Parton-shower effects are found to be marginal in inclusive observables and quite sizeable in observables that are exclusive in additional jet radiation. The Monte Carlo generator presented here allows for realistic experimental effects to be incorporated in state-of-the-art precision analyses of diboson production and of the Higgs boson in the offshell regime.

1 Introduction

One of the main objectives of Run 3 of the Large Hadron Collider (LHC) will be the further investigation of the Higgs sector. Most studies directly targeting the Higgs boson will focus on its onshell production and subsequent decay. Indeed, one might naively expect that the cross section to produce an offshell Higgs boson is negligible, due to the extremely narrow width of the Higgs boson of about 4 MeV in the Standard Model (SM). However, contrary to this expectation, it is known that approximately 10% of $gg \to H^* \to VV$ events are produced with an invariant mass m_{VV} above the $2m_V$ production threshold [1]. The importance of the offshell region for Higgs phenomenology was further highlighted in Ref. [2], which showed that a comparison of onshell and offshell data can provide stringent constraints on the width of the Higgs boson (see also Refs. [3,4]). While later work indicated that such constraints are not model-independent, they also revealed the potential of using offshell data to probe the couplings of the Higgs boson [5–11]. Offshell analyses have been performed by both ATLAS [12,13] and CMS [14–17], and have succeeded in constraining the Higgs boson width to $\mathcal{O}(10\,\text{MeV})$. This is several orders of magnitude smaller than a direct constraint, which is limited by the detector resolution. Nevertheless, offshell analyses are currently still limited by the available statistics. Further studies of offshell Higgs boson production will therefore be a key component of the investigations of the Higgs sector during both Run 3 and in the high luminosity phase of the LHC.

In this paper, we will focus on the production of an offshell Higgs boson through gluon fusion and its subsequent decay into a pair of electroweak gauge bosons. To this end we consider the signal Higgs production process $gg \to H^* \to VV$ together with the corresponding continuum background process $gg \to VV$ and their interference. We study the two diboson modes $VV = \{ZZ, W^+W^-\}$ and we assume leptonic decays of the diboson pair. In the following, for brevity, we often denote the processes according to the intermediate diboson resonances (ZZ, W^+W^-). However by this we always refer to the full four-lepton offshell processes, including the interference between Z and offshell photon production.

The signal process proceeds predominantly through a top-quark loop. For onshell Higgs production, the top-quark mass

[a] e-mail: simone.alioli@unimib.it
[b] e-mail: silvia.ferrarioravasio@physics.ox.ac.uk
[c] e-mail: j.lindert@sussex.ac.uk (corresponding author)
[d] e-mail: raoul.rontsch@cern.ch

is the largest scale in the process and can be approximated as infinitely heavy, allowing this loop-induced process to be reduced to a tree-level one. Using this approximation, the next-to-next-to-next-to-leading order (N3LO) corrections to Higgs production have been computed [18–20]. However, this approximation is not valid for offshell Higgs production, since the virtuality of the Higgs may be comparable to (or even larger than) the top-quark mass. This means that a leading-order (LO) prediction for offshell Higgs production requires the computation of a one-loop amplitude with the full top mass dependence, while the next-to-leading order (NLO) correction requires a two-loop amplitude. By itself, this would not be so onerous, but there is a second reason why predictions for offshell Higgs production are more demanding than for onshell Higgs production. It is well-known that the interference effects between the signal $gg \to H^* \to VV$ and the background process $gg \to VV$ can be sizeable and thus must be taken into account [1]. Moreover, as we discussed above, the impact of top quarks in the loops cannot be neglected, and this means that in the computation of the background amplitudes $gg \to VV$ the contribution from both massless and massive quarks circulating in the loops should be considered. For on-shell Higgs production NLO simulations matched to parton showers are indeed readily available [21,22] without any approximations for the heavy quark loops.

Results for offshell Higgs production including the mass dependence of quarks in the loop and interference effects are known at LO [1,3,4,23]. Results in the presence of an additional radiated jet have also been presented [24,25]. At NLO, the two-loop $gg \to VV$ amplitudes for massless quarks circulating in the loop have been known for several years [26,27], and allow for offshell vector bosons. However, the corresponding amplitudes for massive quark loops have only recently become available [28–30]. We note that these amplitudes treat the vector bosons as being onshell and thus are only valid above the $2m_V$ threshold. Although offshell amplitudes are required for a consistent NLO description in the entire phase-space, the onshell treatment of the vector bosons is not a serious deficiency for offshell Higgs studies. This means that a fully consistent NLO prediction with the exact dependence on the top-quark mass is in sight in this kinematic regime but still not available.

However, NLO calculations including interference effects in $gg \to ZZ$ have been presented based on an expansion in $1/m_t$ [31–33]. This expansion is not valid for high energies, but has been shown to work well below the top-pair production threshold $2m_t$. In fact, Ref. [32] uses a conformal mapping and Padé approximants to extend the results beyond the top-pair threshold. More recently, it has been demonstrated that using an expansion in $1/m_t$ together with a threshold expansion as inputs for Padé approximants can lead to improved estimates for both $gg \to HH$ and $gg \to VV$ amplitudes [34,35]. In Ref. [36] the massive two-loop amplitude for $gg \to ZZ$ has been computed in the high-energy expansion $s, |t| \gg m_t^2$, which opens the door for a NLO description of this process in the phase space $m_{ZZ} > 2m_t$. However, even disregarding these methods, there is a significant region of the offshell phase space with $m_{ZZ} < 2\,m_t$ in which the $1/m_t$ expansion is expected to be reliable, and hence where a good approximation to the NLO corrections can be obtained. We base the Monte Carlo generator for $gg \to ZZ$ presented here on such an approximation, following the calculation of Ref. [33]. Additionally, we employ the reweighting of mass effects in the one-loop amplitudes to estimate the unknown contribution affecting massive two-loop $gg \to ZZ$ amplitudes, which allows us to also cover the region $m_{ZZ} > 2\,m_t$. When considering the $gg \to WW$ process, we only employ the one-loop reweighting procedure. We emphasize that, when the exact massive two-loop amplitudes become available, it will be immediate to extend the generator by replacing these approximate treatments with the exact ones.

Reliable NLO corrections to the continuum background $gg \to VV$ alone can be obtained ignoring heavy quark contributions (or these can be incorporated via a reweighting of the massless two-loop amplitude with the LO mass dependence). They are available in the literature both for $gg \to ZZ$ [37,38] and $gg \to W^+W^-$ [39,40].[1] Formally these are of $\mathcal{O}(\alpha_S^3)$ with respect to the LO $pp \to VV$ process, i.e. they contribute beyond the order of the known NNLO corrections to the quark-induced channels [43–48] - yet they yield phenomenologically relevant contributions.

The NLO results of Refs. [32,33,37–41] are at fixed-order parton level, meaning that they do not account for radiation beyond one additional jet. This, together with the fact that unweighted events are not available, prevents their direct use in event simulations. In this paper, we report on NLO calculations for offshell Higgs production, including interference effects, matched to parton showers using the POWHEG method [49–52]. The implementation extends earlier work by two of us [53] that considered the background process $gg \to ZZ \to 4\ell$ only. Furthermore, in contrast to Ref. [53], here we also include the contribution from qg- and $q\bar{q}$-initiated channels. This implementation allows the generation of unweighted events with additional radiation included through the parton shower, and should facilitate the use of the NLO calculations in experimental analyses. The corresponding POWHEG-BOX-RES generator gg4l will be made publicly available in due time.

[1] The results of Refs. [38,40] also include the offshell Higgs contribution, however without investigating it explicitly. Very recently in Ref. [41] the separation into signal, background and interference has been studied for ZZ production. The latter combined gluon-induced production at NLO with the NNLO corrections to the quark-induced channels, to which NLO EW corrections were also considered [42].

The paper is organized as follows. In Sect. 2, we briefly discuss the technical details involved in the parton-level calculation as well as in the matching procedure. In Sect. 3, we summarize the numerical inputs that we use. In Sect. 4, we present fixed-order results validating our calculation and investigate the applied approximations. Finally in Sect. 5 we present numerical results for ZZ and WW production matched to parton showers. We conclude in Sect. 6.

2 Computational setup

In this section, we describe the matching of the NLO calculation of gluon-induced four-lepton production to parton showers through the POWHEG method implemented in POWHEG-BOX-RES. We first describe the structure of the fixed-order NLO computation and then discuss several details relevant for the matching to PYTHIA 8.

2.1 Structure of the NLO computation

We begin by summarizing the salient features of the NLO calculation, and refer the reader to Ref. [33] for additional discussion. As mentioned in the previous section, we need to consider both Higgs-mediated amplitudes $gg \to H^* \to VV$ as well as continuum production $gg \to VV$ amplitudes. We therefore write the full amplitude for gluon-induced VV production as

$$A = A_{\text{signal}} + A_{\text{bkgd}} \tag{1}$$

where A_{signal} refers to Higgs-mediated amplitudes, while A_{bkgd} refers to amplitudes without any Higgs propagators. Squaring this equation gives

$$|A|^2 = |A_{\text{signal}}|^2 + |A_{\text{bkgd}}|^2 + 2\text{Re}\left(A_{\text{signal}} A^*_{\text{bkgd}}\right). \tag{2}$$

Upon integrating over the phase space for the final state particles, the first two terms on the right-hand side give the signal and background results, respectively, while the third term gives the interference contribution

$$\text{d}\sigma_{\text{full}} = \text{d}\sigma_{\text{signal}} + \text{d}\sigma_{\text{bkgd}} + \text{d}\sigma_{\text{intf}}. \tag{3}$$

In Sects. 4 and 5 we will present results for these contributions separately, as well as for their sum $\text{d}\sigma_{\text{full}}$.

As mentioned in the previous section, the LO amplitudes for both A_{signal} and A_{bkgd} are well known [1,3,4,23,54–56]. At NLO, we have to compute the real and virtual corrections to A_{signal} and A_{bkgd}. The corrections to A_{signal} have been known for some time [57–60]. On the other hand, the NLO corrections to the background amplitude A_{bkgd} are more involved, and deserve a separate discussion.

We begin by examining the virtual corrections to the $gg \to ZZ$ process. In this case, one can clearly separate massless loops of the first five flavours, and massive top-quark loops. The virtual (two-loop) amplitudes for the former are known [26,27], and we construct these using the ggVVamp library [27]. Results for two-loop amplitudes with massive quarks and onshell Z bosons were presented very recently [28,30]. However, here we follow the approach of Refs. [31,33] and use an expansion in $1/m_t$ for the massive amplitudes. This implies that our NLO results for the ZZ production process are only valid below the top pair production threshold $m_{ZZ} < 2m_t$.

An alternative option is to approximate the mass effects of the two-loop amplitudes through a reweighting procedure, using the known one-loop amplitudes. However, contrary to the $1/m_t$ expansion, which is systematically improvable and with a well-defined validity regime, there is no clear indication of how to estimate the accuracy of an approximation in which the virtual amplitude is reweighted using the leading-order mass dependence. Nonetheless, in Sect. 1 we explore this alternative procedure and compare kinematic distributions obtained using the $1/m_t$ expansion to those obtained by reweighting the virtual background amplitude using the exact LO top-mass dependence. As shown there, the reweighting procedure is in excellent agreement with the $1/m_t$ expansion below the $m_{ZZ} < 2m_t$ threshold, and starts to display sizeable differences (up to several percent) above this threshold.

Finally, we need to include double-triangle amplitudes, where each triangle can have either massless or massive quarks in the loop. We employ analytic results for these amplitudes taken from Refs. [61,62].

We now discuss the case of WW production. Since top and bottom quarks mix in the loop, there is no longer a clear division into massive and massless loops. For this reason, Ref. [33] only considered four massless quark flavours in the loop for WW, neglecting the third generation entirely. Here we take a slightly different approach. We compute the two-loop amplitudes $A^{\text{2loop}}_{\text{bkgd}}$ using ggVVamp assuming massless quarks for four active flavours. We then reweight the two-loop helicity amplitude using ratios of massive and massless helicity amplitudes, computed at one-loop:

$$\mathcal{A}^{(2),WW}_{\text{bkgd}} \approx \mathcal{A}^{(2),WW}_{\text{bkgd}}(d,u,s,c) \times \frac{\mathcal{A}^{(1),WW}_{\text{bkgd}}(d,u,s,c,b,\mathbf{t})}{\mathcal{A}^{(1),WW}_{\text{bkgd}}(d,u,s,c)}, \tag{4}$$

where $\mathcal{A}^{(1),WW}_{\text{bkgd}}(d,u,s,c,b,\mathbf{t})$ is the one-loop amplitude at fixed helicity with full mass dependence for the third-generation quarks and $\mathcal{A}^{(1),WW}_{\text{bkgd}}(d,u,s,c)$ the one-loop helicity amplitude with four active flavours.[2] We will comment on the accuracy of this approach in Sect. 4.2.

[2] We note that results for the two-loop $gg \to WW$ amplitudes with massive top quarks and onshell W bosons in the loop were recently presented in Ref. [29].

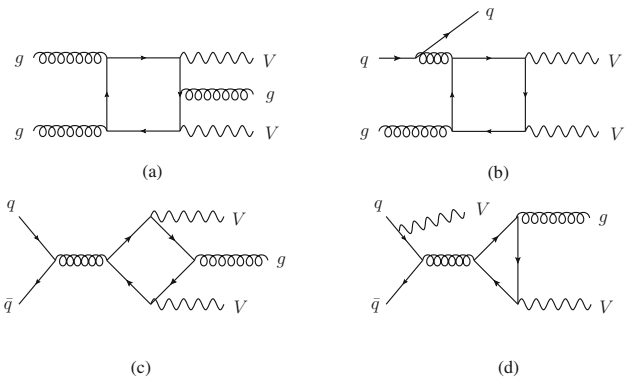

Fig. 1 Real corrections to gluon-induced VV production, with different partonic channels

The real corrections to $gg \to VV$ include both the purely gluonic channel $gg \to VV + g$ as well as channels with initial state quarks $qg \to VV + q$ and $q\bar{q} \to VV + g$ (see Fig. 1) and their crossings. At $\mathcal{O}(\alpha_s^3)$, the former can be unambiguously identified as corrections to the loop-induced process $gg \to VV$. The qg and $q\bar{q}$ channels are more intricate. These channels also appear in the $\mathcal{O}(\alpha_s^3)$ corrections to the $q\bar{q} \to VV$ process, and it is not possible to parametrically distinguish these corrections from the corrections to the loop-induced process that we are interested in. For this reason, these channels were not included in Ref. [33]. On the other hand, there is no obstacle to computing these corrections, as they form a gauge invariant subset and their only infrared singularities are removed through the collinear renormalization of the parton distribution functions. Indeed, results for these channels were included in Refs. [38,40,41]. In this paper, we choose to include these channels in our nominal predictions at NLO and also in the results after matching to the parton shower. At the same time we will also investigate the impact of these channels in Sect. 5.4, so that both their magnitude and their impact on the scale variation can be properly assessed. Note that we define these contributions to include any amplitudes with *at least one* vector boson attached to a closed fermion loop. In particular, amplitudes such as those represented in Fig. 1d (contributing to $gg \to ZZ$) are included.[3]

We compute all the real correction loop-squared amplitudes using `OpenLoops 2` [63,64] including massless and massive quark contributions in the loop, allowing us to retain the full dependence on the top quark mass (and bottom quark mass where applicable). This is in contrast to the approach of Ref. [33] where the real amplitudes for $gg \to ZZ + g$ involving a top-quark loop were computed using an expansion in $1/m_t$. Finally, we note that our calculation includes single-resonant amplitudes in all partonic channels.

In order to ensure numerical stability across the whole phase-space, including in the IR regions close to the soft or collinear limits of the real radiation, we rely on the `OpenLoops` stability system, which automatically reevaluates all phase-space points with the two reduction methods implemented in `Collier` [65]. For unstable points matrix elements are set to zero. We verified that varying the corresponding threshold `stability_kill2` by a factor of 10 around a central value of 10^{-2} leaves all results unchanged (see Ref. [64] for documentation of this threshold parameter).

In order to optimize the treatment of all the colorless resonances, we take advantage of the `POWHEG-BOX-RES` framework [52], which, despite being specifically designed to handle the subtractions when intermediate colored resonances are present, can at the same time improve the phase-space sampling of any resonance. This is achieved by first manually specifying the resonance histories.[4] The `POWHEG-BOX-RES` then decomposes the cross section into contributions associated to a well-defined resonance structure, which are enhanced on that particular cascade chain. Each contribution is separately integrated at this point with a dedicated resonance-aware phase space sampling which makes use of a resonance-aware subtraction procedure. The resonance-aware subtraction makes use of a mapping from a real to the underlying Born configuration that preserves the virtuality of intermediate resonances. Due to the absence of QCD divergences in the resonances, the resonance-aware subtraction is strictly speaking not necessary for the processes considered here. However, we choose to adopt it because its usage improves the statistical errors for observables directly probing the resonance structure. The last essential feature of the `POWHEG-BOX-RES` implementation is the ability to generate remnants and regular events even when the corresponding cross section is negative, which was not possible in previous versions of the `POWHEG-BOX` that were instead assuming them to be positive. Despite usually being squares of matrix elements, in this process remnants and regulars contributions might indeed assume negative values in the calculation of the interference terms. Technical details about necessary modifications in `POWHEG-BOX-RES` to deal with the processes at hand are given in Sect. 1.

2.2 Matching to `PYTHIA 8`

We next discuss the matching of the NLO calculation of $gg \to VV$ to the `PYTHIA 8` parton shower in the framework of `POWHEG-BOX-RES`.

[3] In our code, the user can choose to switch off amplitudes with one vector boson attached to an external quark line using the `ol_noexternalvqq` flag. The user can also turn off the qg and $q\bar{q}$ channels altogether with the `select_real` flag.

[4] The automatic resonance-finding algorithm in `POWHEG-BOX-RES` is not yet able to handle resonances in loop-induced contributions.

The resonance structure that we construct at the partonic level is further preserved by the parton shower by specifying the input resonance cascade chain at the Les Houches event level (LHE) and making sure that the shower does not distort it through recoil effects. This is achieved by using the `PowhegHooks` class in `PYTHIA 8`. However, the `PowhegHooks` class needs to know the number of final state particles involved in the LO process once the resonance decays are stripped. Since in the `POWHEG-BOX-RES` this number is not fixed, we modified the `PowhegHooks` class accordingly, following the recipe adopted in Ref. [66].

The `PYTHIA 8` parton shower implements two recoil schemes for initial-state radiation (ISR): in both cases the recoil is always applied to all final-state particles to absorb the transverse momentum imbalance due to ISR off an initial-initial dipole. In the default scheme [67] the same is also done for initial-final dipoles. There is, however, also the option to use a fully local scheme [68], in which when an initial-state emission takes place from an initial-final dipole, the final-state spectator absorbs the transverse-momentum recoil and the other particles in the event are left unchanged.

The default recoil scheme is the recommended option to handle the s-channel production of colour singlets, while the alternative one was originally designed to handle deep inelastic scattering and vector boson fusion events. Since at LO the process considered in this paper describes the production of a colour singlet, we maintain as our baseline the default recoil scheme of `PYTHIA 8`. However, since in principle we can also generate events with a hard final state jet, in our numerical results we compare the two recoil prescriptions for exclusive observables that might be sensitive to this choice.

In all our showered predictions we include underlying event simulation and hadronization effects. However, in order to simplify the identification of the leptons, we turn off QED radiation and the decay of unstable hadrons.

3 Numerical setup

In this section we present the numerical inputs for the results presented in the following sections.

Coupling and mass input parameters are fixed to the following values:

$$\begin{aligned} m_{\mathrm{Z}} &= 91.1876\ \mathrm{GeV}, & \Gamma_{\mathrm{Z}} &= 2.4952\ \mathrm{GeV}, \\ m_{\mathrm{W}} &= 80.3980\ \mathrm{GeV}, & \Gamma_{\mathrm{W}} &= 2.1054\ \mathrm{GeV}, \\ m_{\mathrm{H}} &= 125.1\ \mathrm{GeV}, & \Gamma_{\mathrm{H}} &= 4.03 \cdot 10^{-3}\ \mathrm{GeV}, \\ m_{\mathrm{t}} &= 173.2\ \mathrm{GeV}, & G_F &= 1.16639 \cdot 10^{-5}\ \mathrm{GeV}^{-2}, \end{aligned}$$

where G_F denotes the Fermi constant and

$$\alpha = \frac{\sqrt{2}}{\pi} m_W \sin^2\theta_W,$$

with the real-valued weak mixing angle

$$\sin^2\theta_W = 1 - \frac{m_W^2}{m_Z^2}.$$

In general, the `gg4l` generator allows for finite bottom-quark masses. In this work, we mostly use the $N_F = 5$ flavour scheme and treat the bottom quark as massless $m_{\mathrm{b}} = 0\ \mathrm{GeV}$. Only in Sect. 4.1, where we validate against the results of Ref. [33], do we use a non-zero bottom-quark mass, and there we choose $m_{\mathrm{b}} = 4.5\ \mathrm{GeV}$.

We use the partonic luminosities and strong coupling from the `NNPDF30_lo_as_0130` and the `NNPDF30_nlo_as_0118` sets [69] for the validation against the results of Ref. [33] that we present in Sect. 4.1. For all other results, we use the `NNPDF31_nlo_as_0118` set [70].

We consider center-of-mass energies of 13 TeV, and set as renormalization and factorization scales for all modes

$$\mu = \mu_R = \mu_F = \frac{m_{4\ell}}{2}, \tag{5}$$

where

$$m_{4\ell}{}^2 = \left(\sum_{i \in \{\ell,\nu\}} p_i \right)^2. \tag{6}$$

We obtain scale uncertainty bands by independently varying the renormalization and factorization scales by a factor of two and omitting antipodal variations.

At the generator level the following kinematic cuts are applied in the ZZ channel,

$$5\ \mathrm{GeV} < m_{\ell\ell} < 180\ \mathrm{GeV}, \tag{7}$$

$$70\ \mathrm{GeV} < m_{4\ell} < 340\ \mathrm{GeV}. \tag{8}$$

We need to impose such an upper cut on $m_{4\ell}$ because, as discussed in the previous sections, the virtual corrections are computed using a $1/m_t$ expansion which is no longer valid for large values of $m_{4\ell}$ [33]. For WW production we only require

$$m_{2\ell 2\nu} > 1\ \mathrm{GeV}, \tag{9}$$

to ensure the renormalization and factorization scales remain inside the perturbative domain. We do not impose any transverse momentum or rapidity requirements on the final-state leptons.

In order to avoid numerical instabilities of the loop-induced amplitudes we need to impose additional mild technical cuts at the generation level. For the Born kinematics, we discard configurations where the transverse momentum of the vector boson is smaller than 100 MeV. For the real corrections, we neglect configurations where the transverse

momentum of the radiated parton is smaller than 100 MeV, as also done in Ref. [53]. Indeed this region only gives rise to power-suppressed contributions that do not significantly change the total cross-section. We verified that our results are independent of these technical cuts varying them by a factor of 5 from 0.1 GeV to 0.5 GeV.

Finally, we reconstruct jets with the anti-k_T algorithm [71] as implemented in the `Fastjet` package [72,73], with jet radius $R = 0.4$ and $p_{T,j} > 20\,\text{GeV}$.

4 Fixed-order NLO results

In the following we present selected fixed-order results that we used to validate our implementation and to investigate the accuracy of the applied approximation for the treatment of mass effects in the virtual corrections.

4.1 Validation

As a validation of our implementation, we compare the fixed-order LO and NLO cross sections for $gg \to ZZ \to e^+e^-\mu^+\mu^-$ and $gg \to W^+W^- \to e^+\nu_e\mu^-\bar{\nu}_\mu$ against the results of Ref. [33] in Table 1, with selection cuts as specified in Ref. [33]. The signal, background and interference contributions are shown separately. Following the approach of Ref. [33], a finite bottom-quark mass m_b is used everywhere in the signal ($|A_{\text{signal}}|^2$). For the ZZ channel, the background ($|A_{\text{bkgd}}|^2$) is computed with $m_b = 0$ and the interference ($2\text{Re}(A_{\text{signal}}A^*_{\text{bkgd}})$) is computed with a finite m_b besides from the virtual contribution which is computed analytically in a mixed-mass scheme, where the bottom mass is neglected in the background amplitude A_{bkgd}.[5] For the WW channel, A_{bkgd} is evaluated with $n_f = 4$, for both the background and the interference channels.

For this validation we do not consider quark-initiated channels in the real contribution, consistent with Ref. [33]. Within numerical accuracy we find convincing agreement between the two calculations at LO and NLO.

4.2 Mass effects

As discussed in Sect. 2.1, the massive contributions to the two-loop virtual amplitudes are incorporated via approximations in our calculation. All other ingredients including the real amplitudes retain full mass dependence. For the ZZ process the approximation for the massive two-loop amplitudes is based on an expansion in $1/m_t$. As discussed in detail in Ref. [33] the resulting accuracy is estimated to be at the percent level for $m_{ZZ} < 2m_t$ and quickly deteriorates beyond this, as shown in Sect. 1. For the WW process we use a reweighting procedure to approximate the massive two-loop amplitudes. As previously mentioned, it is difficult to assess the accuracy of such a procedure. Nevertheless, we will attempt to gauge its impact by comparing against results obtained using only two massless generations for two-loop A_{bkgd} amplitudes, while all other contributions are computed using full mass dependence as usual. We plot these results for the transverse mass m_T of the four lepton system in W^+W^- production in Fig. 2. This observable is defined as

$$m_T = \sqrt{2\,E_{\text{T,miss}}\,p_{\text{T},\ell^+\ell^-}\,(1-\cos(\phi_{\text{miss},\ell^+\ell^-})}, \tag{10}$$

where the missing transverse energy $E_{\text{T,miss}}$ is given by the neutrino momenta at truth level and $\phi_{\text{miss},\ell^+\ell^-}$ is the angle between the sum of the neutrino momenta and the sum of the lepton momenta. For the background contribution the effect of the reweighting is at the few percent level for the bulk of the cross section and increases up to about 15%-20% at large transverse masses. For the interference the impact is at the 15% level inclusively and mildly increases in the tail of the transverse mass distribution. The sum of all contributions – which also includes the signal where no approximations are needed – receives inclusive variations due to the reweighting procedure of 0.7%. In the tail this increases to 10%-15% but also the associate statistical error grows significantly, to the point that it is difficult to reach a firm conclusion.

Table 1 Comparison of LO and NLO cross sections for the signal, background, and interference contributions to $gg \to ZZ \to e^+e^-\mu^+\mu^-$ (top) and $gg \to W^+W^- \to e^+\nu_e\mu^-\bar{\nu}_\mu$ (bottom) with those of Ref. [33]. The qg- or $q\bar{q}$-induced channels are not considered

ZZ: $gg \to e^+e^-\mu^+\mu^-$				
	POWHEG-BOX-RES		Ref. [33]	
Contrib	LO (fb)	NLO (fb)	LO (fb)	NLO (fb)
bkgd	2.898(1)	4.482(6)	2.90(1)	4.49(1)
signal	0.0431(1)	0.0745(2)	0.043(1)	0.074(1)
intf	− 0.1542(3)	− 0.2870(4)	− 0.154(1)	− 0.287(1)
W^+W^-: $gg \to e^+\nu_e\mu^-\bar{\nu}_\mu$				
	POWHEG-BOX-RES		Ref. [33]	
Contrib	LO (fb)	NLO (fb)	LO (fb)	NLO (fb)
bkgd	48.92(6)	74.62(7)	49.0(1)	74.7(1)
signal	48.24(8)	83.31(5)	48.3(1)	83.35(2)
intf	− 2.24(1)	− 4.20(2)	− 2.24(1)	− 4.15(1)

[5] Conversely to the calculation in Ref. [33], we cannot easily use a different bottom mass value for A_{bkgd} and A_{signal} when evaluating the interference using the Born and real matrix elements provided by `OpenLoops`.

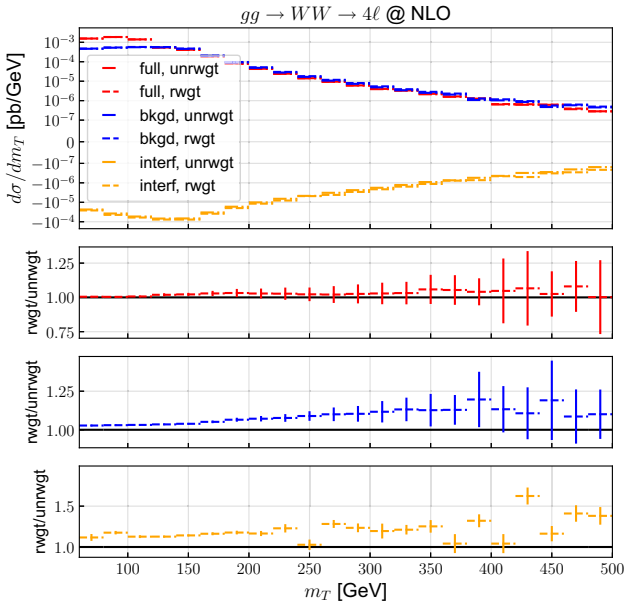

Fig. 2 Differential distribution in the transverse mass m_T of the four lepton system in $gg \to e^+\nu_e\mu^-\bar{\nu}_\mu$ at fixed-order NLO. We show results with and without reweighting of the heavy-quark mass effects in the virtual amplitude using dashed and dashed-dotted curves, respectively. The comparison is shown for the full (red), the background (blue) and the interference (orange) contributions. The lower panels show the bin-by-bin ratios of the results without reweighting to those with reweighting. For the nominal prediction we use a symlog scale with a linear threshold=10^{-7}

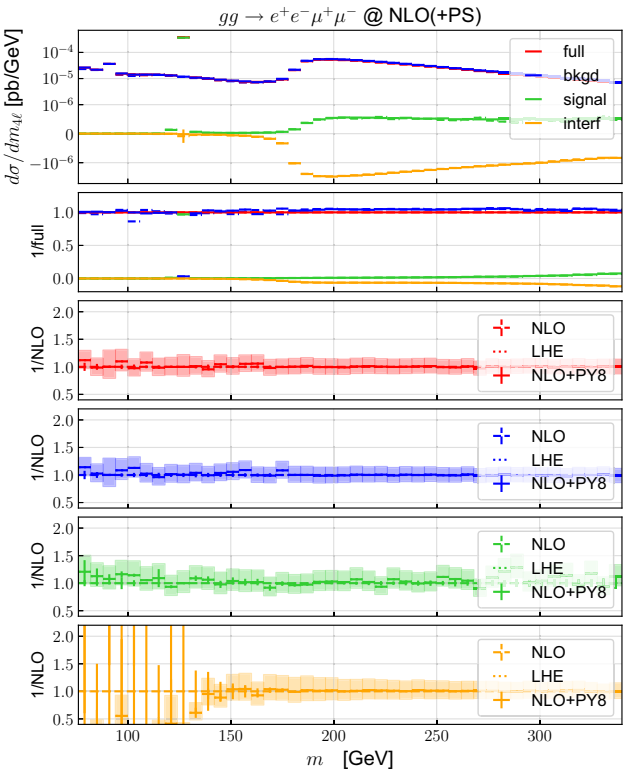

Fig. 3 Differential distribution in invariant mass $m_{4\ell}$ of the four-lepton system in $gg \to e^+e^-\mu^+\mu^-$ at NLO matched to PYTHIA 8. The upper panel shows nominal predictions at fixed-order NLO (dashed) for the background (blue), the signal (green) and the interference (orange) separately and their sum (red) together with NLO+PS predictions (solid). For the nominal prediction we use a symlog scale with a linear threshold=10^{-6}. The first ratio plot shows the relative yield of the different contributions with respect to the full, both at the fixed-order NLO level and also after parton shower. The lower four ratio plots show the LHE level (dotted) and fully showered corrections with respect to fixed-order NLO for the sum of all contributions (second ratio plot), the background only (third ratio plot), the signal only (fourth ratio plot), and for the interference only (fifth ratio plot). The band associated to NLO+PS predictions indicates the 7-point scale variation uncertainty

5 NLO results matched to parton showers

In this section we present our numerical results matched to the PYTHIA 8 parton shower. We consider the different-flavour decay modes $gg \to e^+e^-\mu^+\mu^-$ and $gg \to e^+\nu_e\mu^-\bar{\nu}_\mu$ and for simplicity denote them ZZ and W^+W^- production respectively. The same-flavour leptonic decay modes will also be made available in the gg4l generator, but are not the focus of this study.

5.1 ZZ production

In Figs. 3, 4, 5 and 6 we present numerical results at NLO, LHE level and NLO matched to PYTHIA 8 (NLO+PS) for gluon-induced ZZ production, showing the full result as well as the signal, background and interference contributions separately.

In Fig. 3 the invariant mass of the four-lepton system is shown. The Higgs-mediated signal shows the resonance peak at the Higgs boson mass together with the well-known significant offshell tail. The background clearly exhibits a single-resonant peak at $m_{4\ell} = m_Z$[6] and increases significantly for $m_{4\ell} > 2m_Z$, where both intermediate Z bosons can become onshell. In this region the interference also starts to become relevant. As a consequence of the very inclusive phase-space cuts employed in our numerical analysis, both the signal and the interference reach about 10% of the full result at large $m_{4\ell} \approx 2m_t$, with the interference being destructive. It is well known that the interference provides an even larger destructive contribution at higher values of $m_{4\ell}$, which are however beyond the validity of the $1/mt$ expansion used in our calculation. The $m_{4\ell}$ observable is inclusive in QCD radiation and consequently parton-shower corrections are marginal for all contributions (individually and in their sum). In fact, for

[6] Interestingly we note that this single-resonant peak is absent at LO, as previously pointed out e.g. in Ref. [33]. This is because the

Footnote 6 continued
$gg \to Z^*$ amplitude is proportional to the Z momentum p_Z^μ [61,62], and consequently vanishes when multiplied by the current for the decay $Z^* \to \ell\bar{\ell}\ell'\bar{\ell}'$.

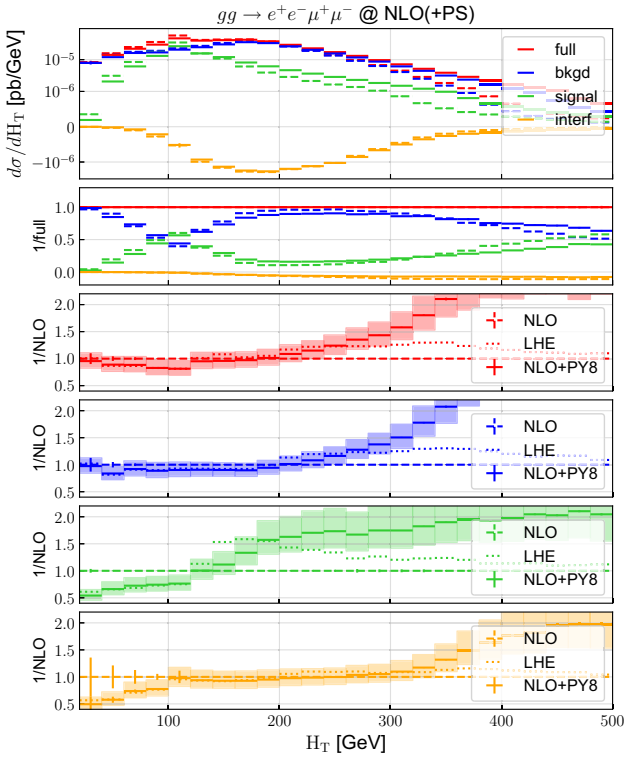

Fig. 4 Differential distribution in H_T in $gg \to e^+e^-\mu^+\mu^-$ at NLO matched to PYTHIA 8. Predictions, colour coding and bands as in Fig. 3

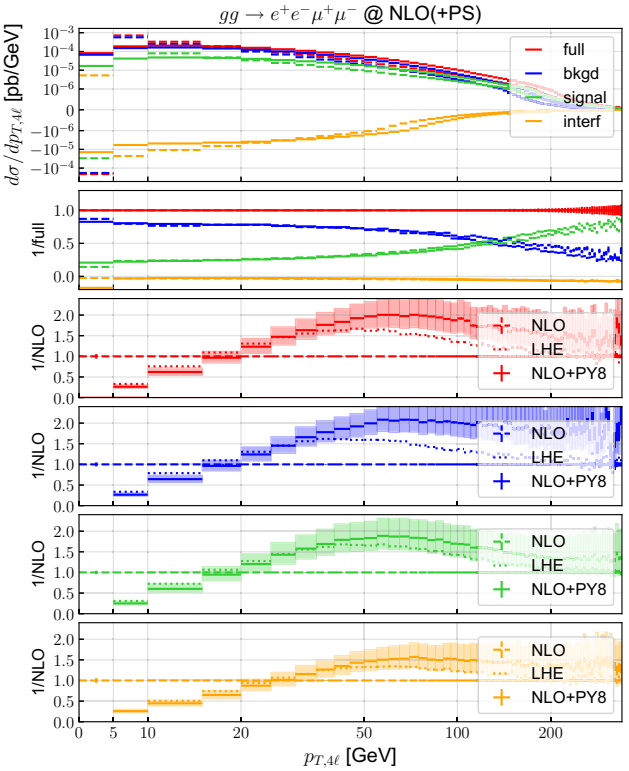

Fig. 5 Differential distribution in the transverse momentum of the four lepton system $p_{T,4\ell}$ in $gg \to e^+e^-\mu^+\mu^-$ matched to PYTHIA 8. Predictions, colour coding and bands as in Fig. 3

all production modes the fixed-order NLO prediction agrees at the percent level with both the LHE level prediction and the fully showered prediction. Scale uncertainties at the fully showered level are approximately 20%. At small invariant masses ($m_{4\ell} < 150$ GeV) the interference becomes very small and consequently Monte Carlo statistics deteriorate quickly in this regime.

Figure 4 shows the distribution in

$$H_T = \sum_{i \in \{\ell, \nu, j\}} p_{T,i}, \tag{11}$$

where the sum over the transverse momenta considers all leptons and reconstructed jets. In this distribution the signal peaks at $H_T = m_H$, while the background peaks at $H_T = 2m_Z$. For small H_T parton-shower corrections are mostly driven by the first radiation already present at the LHE level. For the background contribution, these corrections are small, but for the signal contribution they lead to a negative correction of about 50%. A possible explanation is that the signal distribution is strongly peaked around m_H and therefore very sensitive to additional radiation that moves events away from the peak. For large H_T, the parton showers provide substantial positive corrections up to a factor of 2, while the scale uncertainties can be as large as 50%. This effect can be understood as follows. The upper cut on the invariant mass of the four leptons Eq. (8) also restricts $H_T < 340$ GeV at LO. However, the phase space for $H_T > 340$ GeV can be filled via additional QCD radiation. This leads to significant NLO corrections (not shown here), as well as to sizable parton-shower corrections and LO-like scale uncertainties.

Figures 5 and 6 display the transverse momentum of the four-lepton system and of the hardest jet respectively. For the latter no lower cut on the jet transverse-momentum is applied. The two distributions are identical at fixed-order (they only differ in the first bin which for $p_{T,4\ell}$ includes the Born and virtual contributions proportional to $\delta(p_{T,4\ell})$). The fully showered predictions include a Sudakov suppression which can clearly be seen at the lower end of both the $p_{T,4\ell}$ and the p_{T,j_1} distributions. We also observe that the parton shower changes the sign of the lowest bin in the $p_{T,4\ell}$ spectrum. This can be understood as follows: the virtual contribution, proportional to $\delta(p_{T,4\ell})$, always comes with an opposite sign of the corresponding real contribution.After the shower (and even after the first POWHEG emission) the virtual contribution gets spread out at finite values of $p_{T,4\ell}$. This results in a change of sign in the first bin.

Turning now to the opposite end of the spectrum, the $p_{T,4\ell}$ distribution corresponds to the entire QCD recoil of the four-lepton system and for all contributions receives large parton shower corrections in the tail, while LHE level corrections

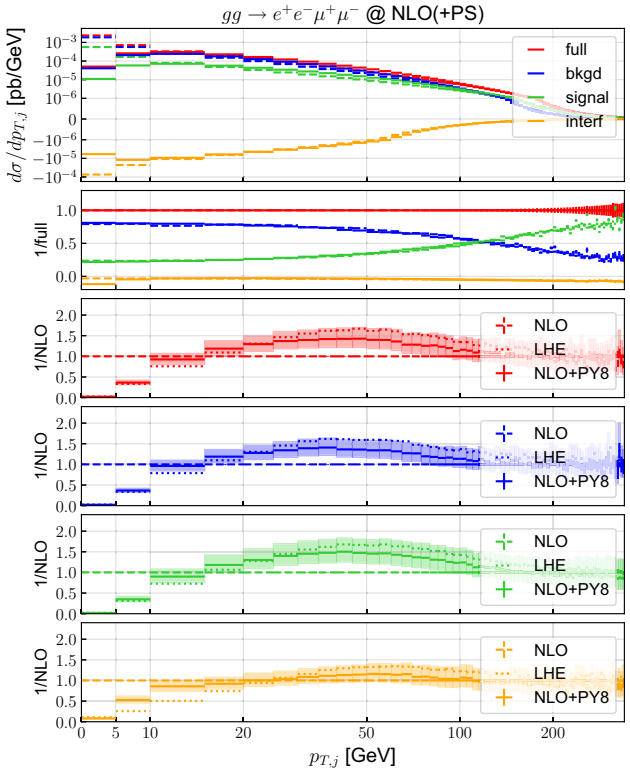

Fig. 6 Differential distribution in the transverse momentum of the hardest jet $p_{\mathrm{T,j_1}}$ in $gg \to e^+e^-\mu^+\mu^-$ at NLO matched to PYTHIA 8. Predictions, colour coding and bands as in Fig. 3

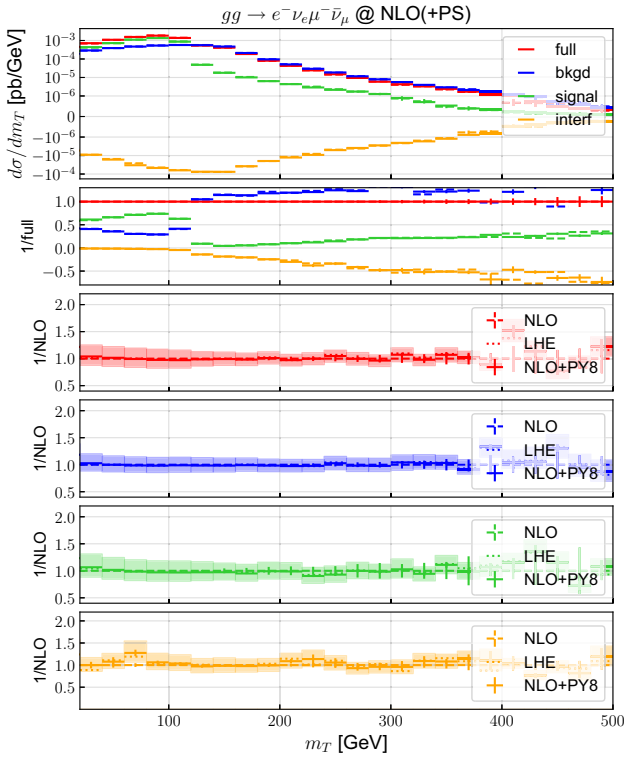

Fig. 7 Differential distribution in transverse mass m_T of the four-lepton system in $gg \to e^+\nu_e\mu^-\bar{\nu}_\mu$ at NLO matched to PYTHIA 8. Predictions, colour coding and bands as in Fig. 3

are largest at $p_{\mathrm{T},4\ell} \approx 40 - 50\,\mathrm{GeV}$ and become small in the tail, where the Sudakov suppression fades away. Similar behaviour was observed for the background contribution studied in Ref. [53]. As already discussed in Ref. [53] the large parton-shower corrections can be explained by the fact that, by adding further radiation, the shower increases the transverse momentum of the colour-neutral four lepton system, which has to recoil against the sum of all emitted particles. The observed large effects are strongly dependent on the employed recoil scheme, as will be discussed in Sect. 5.3. On the contrary, in the tail of $p_{\mathrm{T,j_1}}$ no such enhancement of the corrections due to the parton shower is observed. In fact, by construction the shower emissions are subdominant with respect to the leading jet and on average are separated enough not to be clustered with it. With respect to the LHE level we observe small and negative parton-shower corrections, being compatible within scale uncertainties.

5.2 W^+W^- production

In Figs. 7, 8, 9 and 10 we present numerical results at NLO, LHE level and NLO matched to PYTHIA 8 for gluon-induced W^+W^- production, showing again the signal, background, interference, and full results.

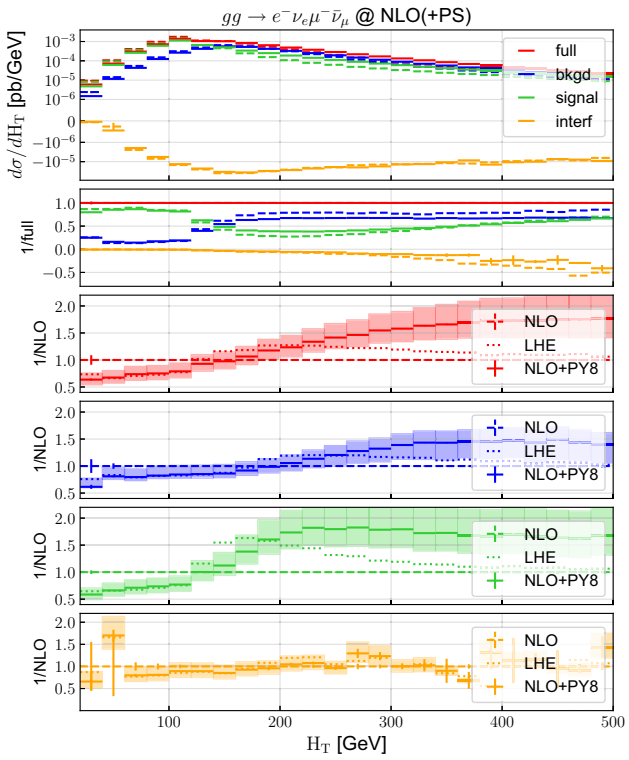

Fig. 8 Differential distribution in H_{T} in $gg \to e^+\nu_e\mu^-\bar{\nu}_\mu$ at NLO matched to PYTHIA 8. Predictions, colour coding and bands as in Fig. 3

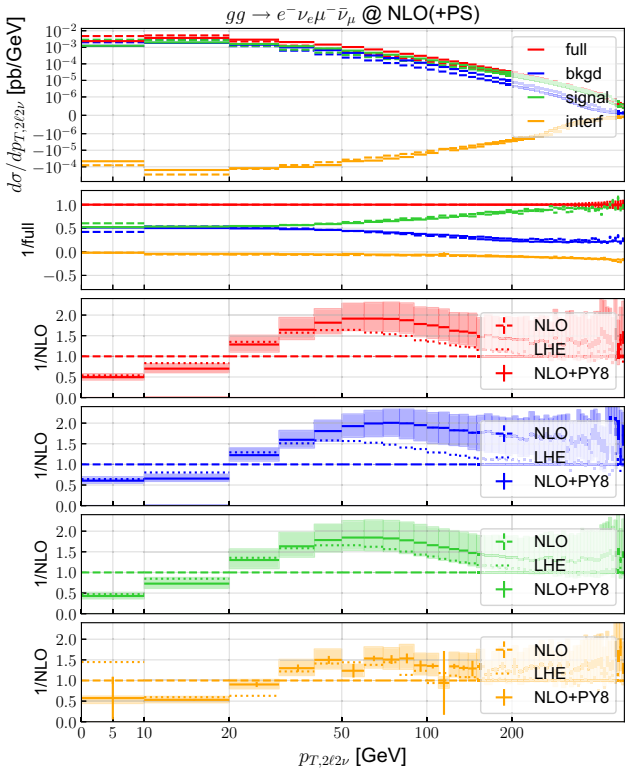

Fig. 9 Differential distribution in the transverse momentum of the four-lepton system $p_{\mathrm{T},2\ell2\nu}$ in $gg \to e^+\nu_e\mu^-\bar{\nu}_\mu$ at NLO matched to PYTHIA 8. Predictions, colour coding and bands as in Fig. 3

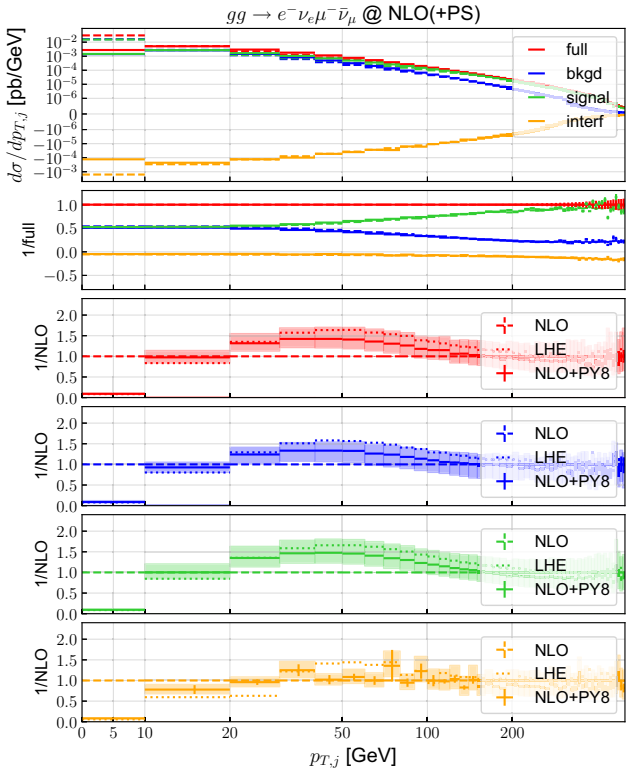

Fig. 10 Differential distribution in the transverse momentum of the hardest jet $p_{\mathrm{T,j_1}}$ in $gg \to e^+\nu_e\mu^-\bar{\nu}_\mu$ at NLO matched to PYTHIA 8. Predictions, colour coding and bands as in Fig. 3

In contrast to the corresponding results for ZZ production, here we consider the distribution in the transverse mass m_T of the four-lepton system, as defined in Eq. (10), instead of the invariant mass of the colour-singlet system. This is shown in Fig. 7. As for the invariant mass in ZZ production, the impact of the parton-shower corrections on the transverse mass in W^+W^- production is marginal, as expected from its inclusive (with respect to QCD radiation) nature. It is noteworthy that the interference becomes very large at high m_T and eventually contributes beyond -50% for $m_T > 300\,\mathrm{GeV}$. However, also for the interference alone parton-shower corrections are marginal for the entire m_T range considered.

A similarly strong enhancement of the interference can also be observed at large H_T, as shown in Fig. 8. In the tail of this observable, parton-shower corrections are again sizable. However in contrast to ZZ production, here no upper boundary on the four-lepton invariant mass is applied and the parton-shower corrections level off for large H_T at around 50% for the background and 70% for the full.

We finally consider the QCD recoil for W^+W^- production in Fig. 9 and the transverse-momentum distribution of the hardest jet in Fig. 10. We observe similar behaviour as for ZZ production: the anticipated Sudakov suppression at the low end of both spectra, very large scheme dependent (see Sect. 5.3 below) parton-shower corrections in the tail of $p_{\mathrm{T},2\ell2\nu}$, and mild corrections in the entire $p_{\mathrm{T,j_1}}$ spectrum.

5.3 Shower recoil scheme

As discussed in Sect. 2.2 PYTHIA 8 implements two alternative shower recoil schemes: the default scheme in which the transverse momentum imbalance after an initial-final dipole emission is democratically distributed among all final-state particles, including the four lepton system, and a fully local scheme, in which the recoil is entirely absorbed by the coloured spectator.[7] In Fig. 11 we compare these two schemes considering the transverse momentum of the four lepton system in the background contribution to ZZ production.

As already anticipated in Sect. 5.1 the default recoil scheme leads to a very hard spectrum in the tail (with a 50% increase with respect to the LHE distribution around 100 GeV). Conversely the dipole scheme remains close to the LHE level at large $p_{T,4\ell}$. For small values of $p_{T,4\ell}$, the dominant contribution should arise from several (soft) emissions whose total transverse momentum sum up to zero. However,

[7] This is activated by the PYTHIA 8 setting `SpaceShower::dipoleRecoil = on`.

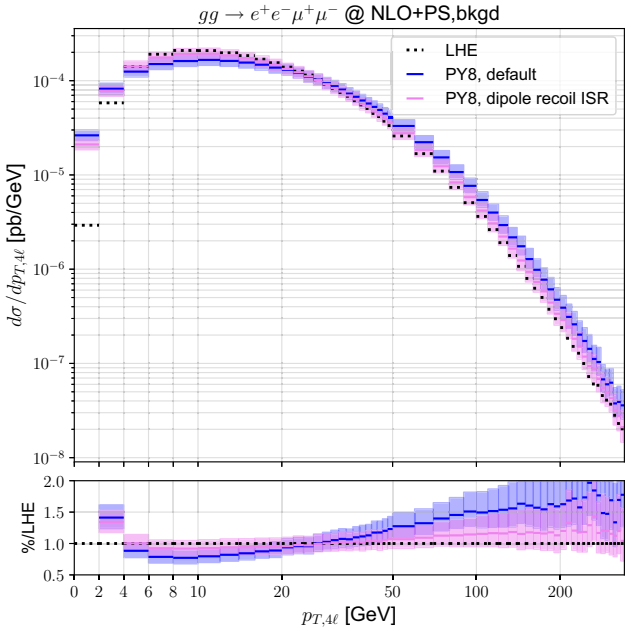

Fig. 11 Differential distribution in transverse momentum of the four charged leptons in $gg \to e^+e^-\mu^+\mu^-$ for the background contribution at the LHE level (black), and at the particle level, using the default PYTHIA 8 recoil (blue) and the fully local dipole recoil (violet). In the lower panel the ratio with respect to the LHE level is shown

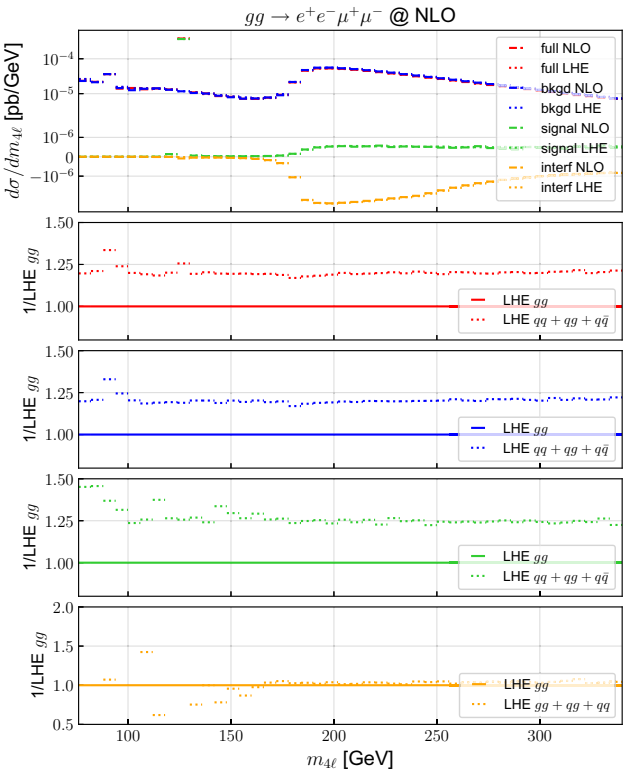

Fig. 12 Differential distribution in invariant mass $m_{4\ell}$ of the four-lepton system in $gg \to e^+e^-\mu^+\mu^-$ at NLO and LHE level. Colour coding of the different production modes as in Fig. 3. The lower ratio plots show the full LHE contribution including all partonic channels ($gg + qg + qq$) over only the gg channel contribution for the different production modes

in the dipole scheme, the transverse momentum recoil for ISR is not always absorbed by the final-state colour singlet. This explains why for very small values of $p_{T,4\ell}$ the local recoil leads to a significantly smaller cross section compared to the default scheme. Indeed if we dress the LO $gg \to VV$ event with multiple soft gluon emissions well separated in rapidity, all the emissions must be independent. However, if we adopt the local recoil, the final-state parton always absorbs the transverse momentum recoil due to emission from an initial-final dipole. This will happen even if the incoming parton is tagged as emitter, and hence even when there is a large angle separation between the final-state spectator and the newly emitted gluon.

Thus, the default scheme yields a better description of the logarithmically enhanced region, while it also overpopulates the hard region of the spectrum. A detailed discussion of the logarithmic accuracy of the parton shower goes beyond the purposes of this article and the choice of the recoil scheme has important implications at higher logarithmic orders [74–79]. However, since the choice of the recoil scheme only affects our predictions beyond the claimed accuracy, a comparison of the two options available in PYTHIA 8 should help assess the size of the total theoretical uncertainty.

5.4 Effect of qg and $q\bar{q}$ channels

In contrast to the calculations in Ref. [33,53], in this study we do include the qg and $q\bar{q}$ induced channels contributing to the real radiation at NLO.[8] Here we would like to explicitly highlight the impact of these production channels. To this end in Figs. 12 and 13 we illustrate at the LHE level the impact of the qg and $q\bar{q}$ channels with respect to only the gg channels for the different production modes, considering the $m_{4\ell}$ and H_{T} distributions in ZZ production. We find very similar results also for the W^+W^- production mode. In the $m_{4\ell}$ distribution the impact of the $qg/q\bar{q}$ channels is rather flat and about 25% for all production modes. For H_{T} it is increasing with increasing H_{T} and reaches up to 50% in the considered range. Clearly, any precision analysis of gg-induced four-lepton production should include these additional partonic channels opening up at NLO.

6 Conclusions and outlook

Gluon-induced four-lepton production offers a unique laboratory for the measurements of offshell Higgs bosons. At the

[8] These channels were also considered in the fixed-order NLO study of [38,40,41].

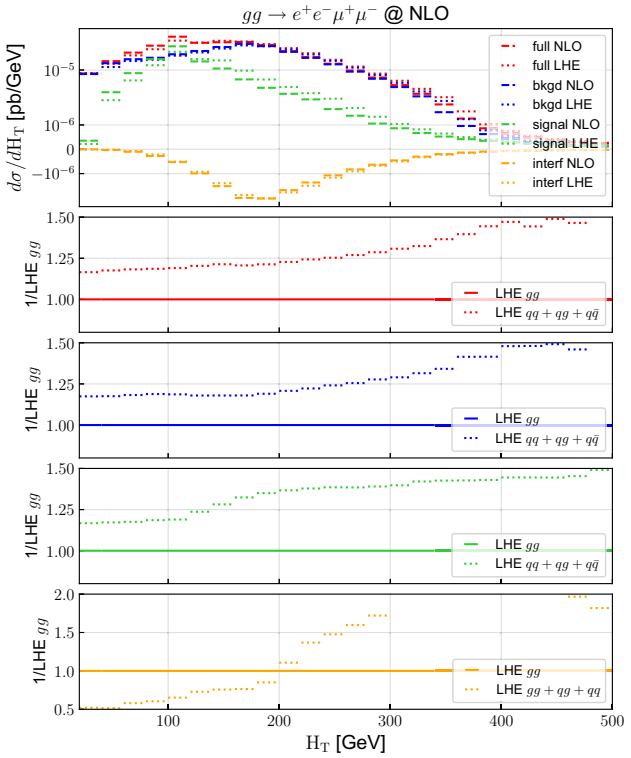

Fig. 13 Differential distribution in H_T in $gg \to e^+e^-\mu^+\mu^-$ at NLO and LHE level. Predictions, colour coding and bands as in Fig. 12

same time precision studies of diboson processes and corresponding background estimates in new physics searches are becoming sensitive to the accuracy of the modeling of the gluon-induced production modes. Having this in mind, in this paper we presented an implementation of the loop-induced processes $gg \to ZZ$ and $gg \to W^+W^-$ including offshell leptonic decays and non-resonant contributions at NLO matched to the PYTHIA 8 parton shower event generator. We consistently include the continuum background contribution, the Higgs-mediated signal, and their interference. All of these are loop-induced processes and therefore their implementation in a fully-exclusive NLO event generator matched to parton showers poses a significant technical challenge.

In inclusive observables, such as the four-lepton invariant-mass distribution in ZZ production, the parton-shower corrections are found to be marginal, while in more exclusive observables like the recoil of the four-lepton system they can become substantial. For the latter we highlighted the importance of the parton-shower recoil scheme. Furthermore we investigated the relevance of the $qg/q\bar{q}$ induced production channels, which partly overlap with the higher-order corrections to quark-induced diboson production.

In our calculation all ingredients have been treated exact at the NLO level apart from the massive amplitudes contributing to the two-loop virtuals, which are incorporated via approximations. Exact results for the latter have become available very recently (albeit for onshell vector bosons) and could be incorporated in an updated version of the gg4l generator presented here. Moreover, the generator will be made publicly available in the POWHEG-BOX-RES framework.

Acknowledgements We are grateful to Fabrizio Caola for useful discussions during the preliminary stages of this work. We also thank Paolo Nason for discussing the modifications to POWHEG-BOX-RES necessary for implementing the processes described in this paper. J.L. is supported by the Science and Technology Research Council (STFC) under the Consolidated Grant ST/T00102X/1 and the STFC Ernest Rutherford Fellowship ST/S005048/1. The work of S.A. is supported by the ERC Starting Grant REINVENT-714788. He also acknowledges funding from Fondazione Cariplo and Regione Lombardia, grant 2017-2070 and by the Italian MUR through the FARE grant R18ZRBEAFC. S.F.R.'s work was supported by the European Research Council (ERC) under the European Union's Horizon 2020 research and innovation programme (grant agreement No. 788223, PanScales) and by the UK Science and Technology Facilities Council (grant number ST/P001246/1).

Data Availability Statement This manuscript has no associated data or the data will not be deposited. [Authors' comment: This is a theoretical study, and results presented are based on calculations and/or simulations.]

Funded by SCOAP[3].

Appendix A: Modifications of the POWHEG-BOX-RES framework

In this section we outline the modifications we implemented to the POWHEG-BOX-RES framework in order to be able to deal with a loop-induced process and with non-positive defined LO processes. These modifications are available in the gg4l process folder and will be incorporated in a future release of the POWHEG-BOX-RES.

As already discussed in Sect. 2, we discard configurations where the one-loop real amplitude becomes unstable, on the ground that this happens only when the p_T of the radiated parton is very small and thus, once we include the subtraction terms, we are left only with negligible power corrections. To do so, setting to zero the amplitude computed in setreal is not sufficient and we have modified the subrou-

tine btildereal to ensure that the subtraction terms are included only when a non-zero real amplitude is found.

For the real corrections, we have the possibility to select only the $gg \to VVg$ channel. By doing so, we are excluding the collinear divergent term $q(\bar{q})g \to VVq(\bar{q})$. Thus, we have modified the subroutine btildecoll to include the integrated $q(\bar{q}) \to gq(\bar{q})$ collinear remnant only when the real $q(\bar{q})g \to VVq(\bar{q})$ contribution is considered.

The NNPDF30_nlo_as_0118 PDF set includes non-perturbative corrections which becomes sizeable for scales smaller than $m_b = 4.5$ GeV. This may cause problems in estimating the upper bound for the strong coupling when generating the radiation according to the method detailed in Ref. [51]. In essence, the upper bound is computed by using the LO running of α_s and a suitable choice of the infrared cutoff $\Lambda_{\rm rad}$, which controls the magnitude of the running, so that

$$\alpha_s^{\rm upb}(p_T) = \frac{1}{2b_0 \log \frac{p_T}{\Lambda_{\rm rad}}} \geq \alpha_s^{\rm cmw}(p_T), \tag{A.1}$$

with $b_0 = \frac{33-2\times 5}{12\pi}$, and "cmw" denoting the Catani–Marchesini–Webber prescription for the running coupling [80]. We have modified the appropriate subroutine (init_rad_lambda) in such a way one spans over scales smaller than the bottom threshold to find the appropriate value of $\Lambda_{\rm rad}$.

When performing event generation, the subroutines in POWHEG-BOX-RES implicitly assume that both the Born and the real squared amplitudes are positive. This is not the case when we consider the interference contribution alone, which can also be negative. Thus, we have modified the subroutines gen_rad_isr, pick_random and do_maxrat to work with absolute values. Furthermore, away from the singular limits, Born and real amplitudes can have opposite signs. When this happens, we always assume that the real contribution is nonsingular and we do not apply any POWHEG Sudakov suppression to it. Therefore we move these nonsingular contributions into the remnants by means of a modified bornzerodamp subroutine.

Appendix B: Approximating heavy-quark mass effects in the two-loop $gg \to ZZ$ amplitudes

As mentioned in the main text, we use an expansion in $1/m_t$ to approximate the massive $gg \to ZZ$ two-loop amplitudes. On the other hand, for offshell WW production, there is no clear separation between massive and massless loops, and the two-loop results are obtained by reweighting, using the known mass dependence at one-loop.

For ZZ production one could in principle adopt a strategy similar to the one use for WW in Eq. (4), by reweighting

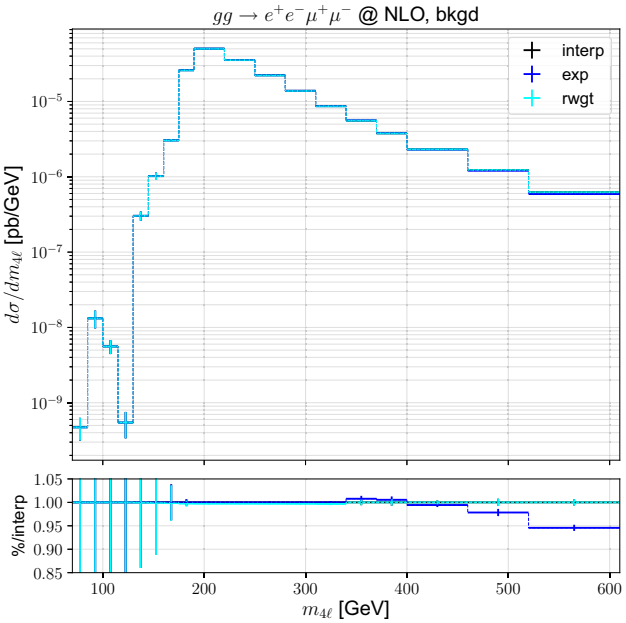

Fig. 14 Differential distribution in invariant mass $m_{4\ell}$ of the four-lepton system in $gg \to e^+e^-\mu^+\mu^-$ at fixed-order NLO for the background contribution. The upper panel shows nominal predictions obtained using different approximations for the two-loop amplitude: $1/m_t$ expansion (exp, blue), reweighting with the exact one-loop amplitude (rwgt, cyan), and an interpolation between the two options (interp, black). The ratio plot shows the relative yield of the different contributions with respect to the interpolated results

$$\mathcal{A}_{\rm bkgd}^{(2),ZZ} \approx \mathcal{A}_{\rm bkgd}^{(2),ZZ}(d,u,s,c,b) \times \frac{\mathcal{A}_{\rm bkgd}^{(1),ZZ}(d,u,s,c,b,\mathbf{t})}{\mathcal{A}_{\rm bkgd}^{(1),ZZ}(d,u,s,c,b)}, \tag{B.2}$$

where the superscripts (1) and (2) indicate one- and two-loop helicity amplitudes respectively, and the bold notation **t** indicates that the top-mass dependence is included exactly, while the non-bold letters denote active flavours. In this appendix we compare this approach with the one we adopted in the main part of this article, *i.e.* the approximation

$$\mathcal{A}_{\rm bkgd}^{(2),ZZ} \approx \mathcal{A}_{\rm bkgd}^{(2),ZZ}(d,u,s,c,b) + \mathcal{A}_{\rm bkgd}^{(2),ZZ,\rm exp}(t), \tag{B.3}$$

where the superscript "exp" denotes the employed $1/m_t$ expansion. We remind the reader that our preference for the results using the expansion is due to the fact that there is no clear, theoretically motivated prescription of estimating the accuracy of the reweighted distributions.

In Figs. 14 and 15 we show results based on the two approximations at fixed order for two inclusive observables, the mass of the ZZ pair ($m_{4\ell}$) and the transverse momentum of the Z boson ($p_{T,\ell^+\ell^-}$), so our findings remain valid also at the NLO+PS level.

In Fig. 14, we note that the reweighted distribution (rwgt, cyan) agrees very well with the calculation performed using

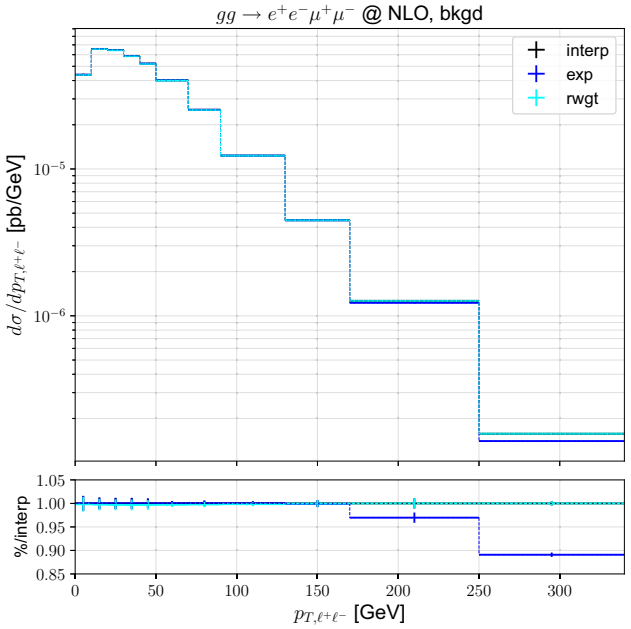

Fig. 15 Differential distribution in transverse momentum $p_{T,\ell^+\ell^-}$ of the dilepton system $\ell^+\ell^- = e^+e^-, \mu^+\mu^-$ in $gg \to e^+e^-\mu^+\mu^-$ at fixed-order NLO for the background contribution. Predictions and colour coding are as in Fig. 14

the $1/m_t$ expansion (exp, blue) for $m_{4\ell} < 340$ GeV, i.e. in the validity regime of the expansion. Interestingly, we observe only a 5% discrepancy between the two distributions in the region 500 GeV $< m_{4\ell} <$ 600 GeV, despite the $1/m_t$ expansion not being justified for such large masses and the reweighting procedure being preferable in this regime. On the other hand, for $m_{4\ell} < 2m_t$ we want to use the results obtained using the $1/m_t$ expansion, whose accuracy is under better control. Consequently we define an additional approximation interpolating smoothly between the reweighted and expanded results. To this end we use an interpolation function $0 < f(m_{4\ell}) < 1$,

$$f(m_{4\ell}) = 1 - \frac{1}{1 + \exp(2m_t - m_{4\ell})}. \tag{B.4}$$

Results obtained using this interpolation (interp) are shown in black in Fig. 14, and are by construction in excellent agreement with the expansion results below the $2m_t$ threshold, and with the reweighted results above it.

In Fig. 15 we observe a similar behaviour for the p_T of the vector boson, with 5% differences between the reweighted and expanded results around $p_{T,\ell^+\ell^-} \approx 200$ GeV, reaching 10% for $p_{T,\ell^+\ell^-} \approx 300$ GeV. The interpolated result, however, shows excellent agreement with the expanded result at low $p_{T,\ell^+\ell^-}$, and with the reweighted result across the distribution. We remind the reader that for events with LO kinematics, there is an upper cutoff $p_{T,\ell^+\ell^-} < m_{4\ell}/2$. Thus, if we require $m_{4\ell} < 340$ GeV, the region $p_{T,\ell^+\ell^-} >$ 170 GeV is populated only by the 4ℓ+jet final state. The different approximations for the treatment of the mass effects in ZZ production including the discussed interpolation are available in the `gg4l` generator via the switch `mass_rwg_frac` to be selected in the `POWHEG` input file.

References

1. N. Kauer, G. Passarino, Inadequacy of zero-width approximation for a light Higgs boson signal. JHEP **08**, 116 (2012). https://doi.org/10.1007/JHEP08(2012)116. arXiv:1206.4803
2. F. Caola, K. Melnikov, Constraining the Higgs boson width with ZZ production at the LHC. Phys. Rev. D **88**, 054024 (2013). https://doi.org/10.1103/PhysRevD.88.054024. arXiv:1307.4935
3. J.M. Campbell, R.K. Ellis, C. Williams, Bounding the Higgs width at the LHC using full analytic results for $gg - > e^-e^+\mu^-\mu^+$. JHEP **04**, 060 (2014). https://doi.org/10.1007/JHEP04(2014)060. arXiv:1311.3589
4. J.M. Campbell, R.K. Ellis, C. Williams, Bounding the Higgs Width at the LHC: Complementary Results from $H \to WW$. Phys. Rev. D **89**(5), 053011 (2014). https://doi.org/10.1103/PhysRevD.89.053011. arXiv:1312.1628
5. I. Anderson, et al., Constraining anomalous HVV interactions at proton and lepton colliders. Phys. Rev. D **89**(3), 035007 (2014). https://doi.org/10.1103/PhysRevD.89.035007. arXiv:1309.4819
6. J.S. Gainer, J. Lykken, K.T. Matchev, S. Mrenna, M. Park, Geolocating the Higgs Boson Candidate at the LHC. Phys. Rev. Lett. **111**, 041801 (2013). https://doi.org/10.1103/PhysRevLett.111.041801. arXiv:1304.4936
7. C. Englert, Y. Soreq, M. Spannowsky, Off-shell Higgs coupling measurements in BSM scenarios. JHEP **05**, 145 (2015). https://doi.org/10.1007/JHEP05(2015)145. arXiv:1410.5440
8. H.E. Logan, Hiding a Higgs width enhancement from off-shell $gg(\to h*) \to ZZ$ measurements. Phys. Rev. D **92**(7), 075038 (2015). https://doi.org/10.1103/PhysRevD.92.075038. arXiv:1412.7577
9. J.S. Gainer, J. Lykken, K.T. Matchev, S. Mrenna, M. Park, Beyond geolocating: constraining higher dimensional operators in $H \to 4\ell$ with off-shell production and more. Phys. Rev. D **91**(3), 035011 (2015). https://doi.org/10.1103/PhysRevD.91.035011. arXiv:1403.4951
10. C. Englert, M. Spannowsky, Limitations and opportunities of off-shell coupling measurements. Phys. Rev. D **90**, 053003 (2014). https://doi.org/10.1103/PhysRevD.90.053003. arXiv:1405.0285
11. A. Azatov, C. Grojean, A. Paul, E. Salvioni, Taming the off-shell Higgs boson, Zh. Eksp. Teor. Fiz. **147**, 410–425 (2015). https://doi.org/10.1134/S1063776115030140. arXiv:1406.6338
12. G. Aad, et al., Constraints on the off-shell Higgs boson signal strength in the high-mass ZZ and WW final states with the ATLAS detector. Eur. Phys. J. C **75**(7), 335 (2015). https://doi.org/10.1140/epjc/s10052-015-3542-2. arXiv:1503.01060
13. M. Aaboud, et al., Constraints on off-shell Higgs boson production and the Higgs boson total width in $ZZ \to 4\ell$ and $ZZ \to 2\ell 2\nu$ final states with the ATLAS detector. Phys. Lett. B **786**, 223–244 (2018). https://doi.org/10.1016/j.physletb.2018.09.048. arXiv:1808.01191
14. V. Khachatryan, et al., Constraints on the Higgs boson width from off-shell production and decay to Z-boson pairs. Phys. Lett. B **736**, 64–85 (2014). https://doi.org/10.1016/j.physletb.2014.06.077. arXiv:1405.3455
15. V. Khachatryan, et al., Limits on the Higgs boson lifetime and width from its decay to four charged leptons. Phys. Rev.

D **92**(7), 072010 (2015). https://doi.org/10.1103/PhysRevD.92.072010. arXiv:1507.06656
16. V. Khachatryan, et al., Search for Higgs boson off-shell production in proton-proton collisions at 7 and 8 TeV and derivation of constraints on its total decay width. JHEP **09**, 051 (2016). https://doi.org/10.1007/JHEP09(2016)051. arXiv:1605.02329
17. A.M. Sirunyan, et al., Measurements of the Higgs boson width and anomalous HVV couplings from on-shell and off-shell production in the four-lepton final state. Phys. Rev. D **99**(11), 112003 (2019). https://doi.org/10.1103/PhysRevD.99.112003. arXiv:1901.00174
18. C. Anastasiou, C. Duhr, F. Dulat, F. Herzog, B. Mistlberger, Higgs boson gluon-fusion production in QCD at three loops. Phys. Rev. Lett. **114**, 212001 (2015). https://doi.org/10.1103/PhysRevLett.114.212001. arXiv:1503.06056
19. C. Anastasiou, C. Duhr, F. Dulat, E. Furlan, T. Gehrmann, F. Herzog, A. Lazopoulos, B. Mistlberger, High precision determination of the gluon fusion Higgs boson cross-section at the LHC. JHEP **05**, 058 (2016). https://doi.org/10.1007/JHEP05(2016)058. arXiv:1602.00695
20. B. Mistlberger, Higgs boson production at hadron colliders at N^3LO in QCD. JHEP **05**, 028 (2018). https://doi.org/10.1007/JHEP05(2018)028. arXiv:1802.00833
21. E. Bagnaschi, G. Degrassi, P. Slavich, A. Vicini, Higgs production via gluon fusion in the POWHEG approach in the SM and in the MSSM. JHEP **02**, 088 (2012). https://doi.org/10.1007/JHEP02(2012)088. arXiv:1111.2854
22. H. Mantler, M. Wiesemann, Hadronic Higgs production through NLO + PS in the SM, the 2HDM and the MSSM. Eur. Phys. J. C **75**(6), 257 (2015). https://doi.org/10.1140/epjc/s10052-015-3462-1. arXiv:1504.06625
23. T. Binoth, N. Kauer, P. Mertsch, Gluon-induced QCD corrections to pp → ZZ → l anti-l l-prime anti-l-prime, in: 16th International Workshop on Deep Inelastic Scattering and Related Subjects, p. 142 (2008). https://doi.org/10.3360/dis.2008.142. arXiv:0807.0024
24. F. Cascioli, S. Höche, F. Krauss, P. Maierhöfer, S. Pozzorini, F. Siegert, Precise Higgs-background predictions: merging NLO QCD and squared quark-loop corrections to four-lepton + 0,1 jet production. JHEP **01**, 046 (2014). https://doi.org/10.1007/JHEP01(2014)046. arXiv:1309.0500
25. J.M. Campbell, R.K. Ellis, E. Furlan, R. Röntsch, Interference effects for Higgs boson mediated Z-pair plus jet production. Phys. Rev. D **90**(9), 093008 (2014). https://doi.org/10.1103/PhysRevD.90.093008. arXiv:1409.1897
26. F. Caola, J.M. Henn, K. Melnikov, A.V. Smirnov, V.A. Smirnov, Two-loop helicity amplitudes for the production of two off-shell electroweak bosons in gluon fusion. JHEP **06**, 129 (2015). https://doi.org/10.1007/JHEP06(2015)129. arXiv:1503.08759
27. A. von Manteuffel, L. Tancredi, The two-loop helicity amplitudes for $gg \to V_1V_2 \to 4$ leptons. JHEP **06**, 197 (2015). https://doi.org/10.1007/JHEP06(2015)197. arXiv:1503.08835
28. B. Agarwal, S.P. Jones, A. von Manteuffel, Two-loop helicity amplitudes for $gg \to ZZ$ with full top-quark mass effects. arXiv:2011.15113
29. C. Brønnum-Hansen, C.-Y. Wang, Contribution of third generation quarks to two-loop helicity amplitudes for W boson pair production in gluon fusion. https://doi.org/10.1007/JHEP01(2021)170. arXiv:2009.03742
30. C. Brønnum-Hansen, C.-Y. Wang, Top quark contribution to two-loop helicity amplitudes for Z boson pair production in gluon fusion. arXiv:2101.12095
31. K. Melnikov, M. Dowling, Production of two Z-bosons in gluon fusion in the heavy top quark approximation. Phys. Lett. B **744**, 43–47 (2015). https://doi.org/10.1016/j.physletb.2015.03.030. arXiv:1503.01274
32. J.M. Campbell, R.K. Ellis, M. Czakon, S. Kirchner, Two loop correction to interference in $gg \to ZZ$. JHEP **08**, 011 (2016). https://doi.org/10.1007/JHEP08(2016)011. arXiv:1605.01380
33. F. Caola, M. Dowling, K. Melnikov, R. Rontsch, L. Tancredi, QCD corrections to vector boson pair production in gluon fusion including interference effects with off-shell Higgs at the LHC. JHEP **07**, 087 (2016). https://doi.org/10.1007/JHEP07(2016)087. arXiv:1605.04610
34. R. Gröber, A. Maier, T. Rauh, Reconstruction of top-quark mass effects in Higgs pair production and other gluon-fusion processes. JHEP **03**, 020 (2018). https://doi.org/10.1007/JHEP03(2018)020. arXiv:1709.07799
35. R. Gröber, A. Maier, T. Rauh, Top quark mass effects in $gg \to ZZ$ at two loops and off-shell Higgs boson interference. Phys. Rev. D **100**(11), 114013 (2019). https://doi.org/10.1103/PhysRevD.100.114013. arXiv:1908.04061
36. J. Davies, G. Mishima, M. Steinhauser, D. Wellmann, gg→ZZ: analytic two-loop results for the low- and high-energy regions. JHEP **04**, 024 (2020). https://doi.org/10.1007/JHEP04(2020)024. arXiv:2002.05558
37. F. Caola, K. Melnikov, R. Röntsch, L. Tancredi, QCD corrections to ZZ production in gluon fusion at the LHC. Phys. Rev. D **92**(9), 094028 (2015). https://doi.org/10.1103/PhysRevD.92.094028. arXiv:1509.06734
38. M. Grazzini, S. Kallweit, M. Wiesemann, J.Y. Yook, ZZ production at the LHC: NLO QCD corrections to the loop-induced gluon fusion channel. JHEP **03**, 070 (2019). https://doi.org/10.1007/JHEP03(2019)070. arXiv:1811.09593
39. F. Caola, K. Melnikov, R. Röntsch, L. Tancredi, QCD corrections to W^+W^- production through gluon fusion. Phys. Lett. B **754**, 275–280 (2016). https://doi.org/10.1016/j.physletb.2016.01.046. arXiv:1511.08617
40. M. Grazzini, S. Kallweit, M. Wiesemann, J. Y. Yook, W^+W^- production at the LHC: NLO QCD corrections to the loop-induced gluon fusion channel. Phys. Lett. B **804**, 135399 (2020). https://doi.org/10.1016/j.physletb.2020.135399. arXiv:2002.01877
41. M. Grazzini, S. Kallweit, M. Wiesemann, J.Y. Yook, Four lepton production in gluon fusion: off-shell Higgs effects in NLO QCD. arXiv:2102.08344
42. M. Grazzini, S. Kallweit, J. M. Lindert, S. Pozzorini, M. Wiesemann, NNLO QCD + NLO EW with Matrix+OpenLoops: precise predictions for vector-boson pair production. JHEP **02**, 087 (2020). https://doi.org/10.1007/JHEP02(2020)087. arXiv:1912.00068
43. F. Cascioli, T. Gehrmann, M. Grazzini, S. Kallweit, P. Maierhöfer, A. von Manteuffel, S. Pozzorini, D. Rathlev, L. Tancredi, E. Weihs, ZZ production at hadron colliders in NNLO QCD. Phys. Lett. B **735**, 311–313 (2014). https://doi.org/10.1016/j.physletb.2014.06.056. arXiv:1405.2219
44. T. Gehrmann, M. Grazzini, S. Kallweit, P. Maierhöfer, A. von Manteuffel, S. Pozzorini, D. Rathlev, L. Tancredi, W^+W^- production at hadron colliders in next to next to leading order QCD. Phys. Rev. Lett. **113**(21), 212001 (2014). https://doi.org/10.1103/PhysRevLett.113.212001. arXiv:1408.5243
45. M. Grazzini, S. Kallweit, D. Rathlev, ZZ production at the LHC: fiducial cross sections and distributions in NNLO QCD. Phys. Lett. B **750**, 407–410 (2015). https://doi.org/10.1016/j.physletb.2015.09.055. arXiv:1507.06257
46. M. Grazzini, S. Kallweit, S. Pozzorini, D. Rathlev, M. Wiesemann, W^+W^- production at the LHC: fiducial cross sections and distributions in NNLO QCD. JHEP **08**, 140 (2016). https://doi.org/10.1007/JHEP08(2016)140. arXiv:1605.02716
47. G. Heinrich, S. Jahn, S. Jones, M. Kerner, J. Pires, NNLO predictions for Z-boson pair production at the LHC. JHEP **03**, 142 (2018). https://doi.org/10.1007/JHEP03(2018)142. arXiv:1710.06294
48. S. Kallweit, M. Wiesemann, ZZ production at the LHC: NNLO predictions for $2\ell 2\nu$ and 4ℓ signatures. Phys. Lett. B **786**,

382–389 (2018). https://doi.org/10.1016/j.physletb.2018.10.016. arXiv:1806.05941
49. P. Nason, A new method for combining NLO QCD with shower Monte Carlo algorithms. JHEP **11**, 040 (2004). https://doi.org/10.1088/1126-6708/2004/11/040. arXiv:hep-ph/0409146
50. S. Frixione, P. Nason, C. Oleari, Matching NLO QCD computations with Parton Shower simulations: the POWHEG method. JHEP **11**, 070 (2007). https://doi.org/10.1088/1126-6708/2007/11/070. arXiv:0709.2092
51. S. Alioli, P. Nason, C. Oleari, E. Re, A general framework for implementing NLO calculations in shower Monte Carlo programs: the POWHEG BOX. JHEP **06**, 043 (2010). https://doi.org/10.1007/JHEP06(2010)043. arXiv:1002.2581
52. T. Ježo, P. Nason, On the treatment of resonances in next-to-leading order calculations matched to a parton shower. JHEP **12**, 065 (2015). https://doi.org/10.1007/JHEP12(2015)065. arXiv:1509.09071
53. S. Alioli, F. Caola, G. Luisoni, R. Röntsch, ZZ production in gluon fusion at NLO matched to parton-shower. Phys. Rev. D **95**(3), 034042 (2017). https://doi.org/10.1103/PhysRevD.95.034042. arXiv:1609.09719
54. E. Glover, J. van der Bij, Z Boson pair production via gluon fusion. Nucl. Phys. B **321**, 561–590 (1989). https://doi.org/10.1016/0550-3213(89)90262-9
55. T. Matsuura, J. van der Bij, Characteristics of leptonic signals for Z boson pairs at hadron colliders. Z. Phys. C **51**, 259–266 (1991). https://doi.org/10.1007/BF01475793
56. C. Zecher, T. Matsuura, J. van der Bij, Leptonic signals from off-shell Z boson pairs at hadron colliders. Z. Phys. C **64**, 219–226 (1994). https://doi.org/10.1007/BF01557393. arXiv:hep-ph/9404295
57. R. Ellis, I. Hinchliffe, M. Soldate, J. van der Bij, Higgs decay to tau+ tau−: a possible signature of intermediate mass Higgs bosons at the SSC. Nucl. Phys. B **297**, 221–243 (1988). https://doi.org/10.1016/0550-3213(88)90019-3
58. M. Spira, A. Djouadi, D. Graudenz, P. Zerwas, Higgs boson production at the LHC. Nucl. Phys. B **453**, 17–82. https://doi.org/10.1016/0550-3213(95)00379-7. arXiv:hep-ph/9504378
59. R. Harlander, P. Kant, Higgs production and decay: analytic results at next-to-leading order QCD. JHEP **12**, 015 (2005). https://doi.org/10.1088/1126-6708/2005/12/015. arXiv:hep-ph/0509189
60. U. Aglietti, R. Bonciani, G. Degrassi, A. Vicini, Analytic results for virtual QCD corrections to Higgs production and decay. JHEP **01**, 021 (2007). https://doi.org/10.1088/1126-6708/2007/01/021. arXiv:hep-ph/0611266
61. K. Hagiwara, T. Kuruma, Y. Yamada, Three jet distributions from the one loop Z g g vertex at e+ e− colliders. Nucl. Phys. B **358**, 80–96 (1991). https://doi.org/10.1016/0550-3213(91)90532-3
62. J. M. Campbell, R. Ellis, G. Zanderighi, Next-to-leading order predictions for $WW + 1$ jet distributions at the LHC. JHEP **12**, 056 (2007). https://doi.org/10.1088/1126-6708/2007/12/056. arXiv:0710.1832
63. F. Cascioli, P. Maierhofer, S. Pozzorini, scattering amplitudes with open loops. Phys. Rev. Lett. **108**, 111601 (2012). https://doi.org/10.1103/PhysRevLett.108.111601. arXiv:1111.5206
64. F. Buccioni, J.-N. Lang, J. M. Lindert, P. Maierhöfer, S. Pozzorini, H. Zhang, M. F. Zoller, OpenLoops 2. Eur. Phys. J. C **79**(10), 866 (2019). https://doi.org/10.1140/epjc/s10052-019-7306-2. arXiv:1907.13071
65. A. Denner, S. Dittmaier, L. Hofer, Collier: a fortran-based Complex One-Loop LIbrary in Extended Regularizations. Comput. Phys. Commun. **212**, 220–238 (2017). https://doi.org/10.1016/j.cpc.2016.10.013. arXiv:1604.06792
66. S. Ferrario Ravasio, T. Ježo, P. Nason, C. Oleari, A theoretical study of top-mass measurements at the LHC using NLO+PS generators of increasing accuracy. Eur. Phys. J. C **78**(6), 458 (2018) [Addendum: Eur. Phys. J. C **79**, 859 (2019)]. https://doi.org/10.1140/epjc/s10052-019-7336-9. arXiv:1906.09166
67. T. Sjostrand, P.Z. Skands, Transverse-momentum-ordered showers and interleaved multiple interactions. Eur. Phys. J. C **39**, 129–154 (2005). https://doi.org/10.1140/epjc/s2004-02084-y. arXiv:hep-ph/0408302
68. B. Cabouat, T. Sjöstrand, Some dipole shower studies. Eur. Phys. J. C **78**(3), 226 (2018). https://doi.org/10.1140/epjc/s10052-018-5645-z. arXiv:1710.00391
69. R.D. Ball et al., Parton distributions for the LHC Run II. JHEP **04**, 040 (2015). https://doi.org/10.1007/JHEP04(2015)040. arXiv:1410.8849
70. R.D. Ball, et al., Parton distributions from high-precision collider data. Eur. Phys. J. C **77**(10), 663 (2017). https://doi.org/10.1140/epjc/s10052-017-5199-5. arXiv:1706.00428
71. M. Cacciari, G.P. Salam, G. Soyez, The anti-k_t jet clustering algorithm. JHEP **04**, 063 (2008). https://doi.org/10.1088/1126-6708/2008/04/063. arXiv:0802.1189
72. M. Cacciari, G.P. Salam, Dispelling the N^3 myth for the k_t jet-finder. Phys. Lett. B **641**, 57–61 (2006). https://doi.org/10.1016/j.physletb.2006.08.037. arXiv:hep-ph/0512210
73. M. Cacciari, G. P. Salam, G. Soyez, FastJet User Manual. Eur. Phys. J. C **72**, 1896 (2012). https://doi.org/10.1140/epjc/s10052-012-1896-2. arXiv:1111.6097
74. Z. Nagy, D. E. Soper, On the transverse momentum in Z-boson production in a virtuality ordered parton shower. JHEP **03**, 097 (2010). https://doi.org/10.1007/JHEP03(2010)097. arXiv:0912.4534
75. M. Dasgupta, F.A. Dreyer, K. Hamilton, P.F. Monni, G.P. Salam, Logarithmic accuracy of parton showers: a fixed-order study. JHEP **09**, 033 (2018) [Erratum: JHEP **03**, 083 (2020)]. https://doi.org/10.1007/JHEP09(2018)033. arXiv:1805.09327
76. G. Bewick, S. Ferrario Ravasio, P. Richardson, M.H. Seymour, Logarithmic accuracy of angular-ordered parton showers. JHEP **04**, 019 (2020). https://doi.org/10.1007/JHEP04(2020)019. arXiv:1904.11866
77. M. Dasgupta, F.A. Dreyer, K. Hamilton, P.F. Monni, G.P. Salam, G. Soyez, Parton showers beyond leading logarithmic accuracy. Phys. Rev. Lett. **125**(5), 052002 (2020). https://doi.org/10.1103/PhysRevLett.125.052002. arXiv:2002.11114
78. J.R. Forshaw, J. Holguin, S. Plätzer, Building a consistent parton shower. JHEP **09**, 014 (2020). https://doi.org/10.1007/JHEP09(2020)014. arXiv:2003.06400
79. K. Hamilton, R. Medves, G.P. Salam, L. Scyboz, G. Soyez, Colour and logarithmic accuracy in final-state parton showers. arXiv:2011.10054
80. S. Catani, B.R. Webber, G. Marchesini, QCD coherent branching and semiinclusive processes at large x. Nucl. Phys. B **349**, 635–654 (1991). https://doi.org/10.1016/0550-3213(91)90390-J